

Giant tunability of exciton photoluminescence emission in antiferromagnetic EuTe

W. Heiss,* G. Prechtl, and G. Springholz

Institut für Halbleiter- und Festkörperphysik, Johannes Kepler Universität, A-4040 Linz, Austria

(Received 16 November 2000; published 5 April 2001)

The photoluminescence properties of antiferromagnetic EuTe layers grown by molecular-beam epitaxy are reported. At low temperatures, two excitonic photoluminescence peaks are observed at 1.92 and 1.88 eV with a full width at half maximum of about 10 meV. With applied magnetic field, these excitonic transitions shift linearly by -34 meV/T to smaller transition energies with a total shift of more than 240 meV at 7.2 T. This is the largest tuning range observed in any semiconductor. The observed magnetic field and temperature dependence of the luminescence lines is explained by the formation of large magnetic polarons due to exchange interactions between the d -like electrons in the conduction band and localized $4f$ spins.

DOI: 10.1103/PhysRevB.63.165323

PACS number(s): 78.40.Fy, 78.20.Ls, 78.55.-m, 78.66.Li

I. INTRODUCTION

Solid-state electronic devices for spin polarization control of free carriers¹⁻³ have attracted tremendous interest because of their great potential for realization of spin electronics and quantum computation. One of the key elements of such devices are magnetic or semimagnetic semiconductors that exhibit strong exchange interactions between free carriers and localized magnetic moments, with strengths much larger than in metals. This leads to a drastic enhancement of the free carrier spin (Zeeman) splitting⁴ and to the formation of magnetic polarons (MP) (Refs. 5-7) due to the ferromagnetic alignment of the localized spins within the Bohr radius of the free carriers. Usually, these effects are most pronounced in paramagnetic diluted magnetic semiconductors (DMS) where the excitons are extended over several sites of magnetic ions. Although in antiferromagnetic semiconductors or insulators such as MnF₂ the concentration of magnetic ions is much larger than in DMS, the carriers created, e.g., by photoexcitation are usually strongly localized (Frenkel excitons).⁸ This minimizes the interaction between the carriers and the localized magnetic moments, and therefore a significant enhancement of the spin splitting or the formation of extended magnetic polarons does not occur.

In the present work, we have investigated the unique magneto-optical properties of EuTe, which belongs to the class of wide-band-gap magnetic semiconductors. The Eu-monochalcogenides (EuX) are classical Heisenberg magnets due to exchange interactions between the localized magnetic moments of the half-filled Eu²⁺ $4f$ levels (spin $\frac{7}{2}$). Because of the opposite sign of the nearest- and next-nearest-neighbor exchange integral, EuTe is antiferromagnetic of type-II structure. In contrast to other wide-band-gap antiferromagnets, in EuTe, photoexcitation creates excitons of *extended electrons* in the conduction band formed by the Eu²⁺ $5d$ and $6s$ orbitals, and *strongly localized holes* within the half-filled Eu²⁺ $4f$ levels. These $4f$ levels are located in between the conduction and the valence band, where the latter is formed by the p orbitals of the chalcogenes. While all previous optical studies of EuTe performed on powders,⁹ polycrystalline thin layers,¹⁰ or bulk crystals^{9,11} showed only a very broad luminescence at transition energies around 1.5 eV, we find

that high-purity epitaxial EuTe layers grown by molecular-beam epitaxy exhibit very narrow excitonic photoluminescence (PL) lines at about 1.9 eV that have not been observed in previous studies. These excitonic lines exhibit a giant magnetic-field tunability by more than 240 meV for magnetic fields between 0 and 7.2 T, with an essentially constant tuning slope of 34 meV/T. This is by far the largest value observed in any semiconductor and corresponds to an effective g factor as large as 1140. A detailed analysis of the experimental data shows that unlike the paramagnetic DMS, where the magnetic-field-induced redshift of the PL emission is dominated by the exciton Zeeman splitting, the huge tunability in EuTe is due to d - f exchange interaction between the “semilocalized” excitons and the localized magnetic moments of the Eu²⁺ ions, which results in the formation of large magnetic polarons.

II. EXPERIMENT

The EuTe samples studied in the present work were grown in a Riber 1000 molecular-beam-epitaxy (MBE) system onto (111) oriented BaF₂ substrates, using elemental effusion cells for Eu and Te as beam flux sources. BaF₂ has the cubic calcium-fluoride crystal structure and its lattice constant deviates only by 6% from that of EuTe. In addition, the thermal-expansion coefficient of BaF₂ is well matched to that of EuTe, which prevents the buildup of high thermal strains during cooling to cryogenic temperatures. From *in situ* reflection high-energy electron-diffraction (RHEED) studies, we find that the EuTe (111) surface shows a very strong tendency for (100) facetation due to the resulting lowering of the free-surface energy. Therefore, two-dimensional (2D) layer-by-layer growth can be obtained only under precisely controlled growth conditions where the growing surface is kept close to the transition between the Eu- and Te-stabilized surface state.¹² These surface states can be easily distinguished by *in situ* RHEED because of their different surface reconstructions (see Ref. 12). Under such conditions, all epitaxial films show sharply streaked RHEED diffraction patterns throughout MBE growth and exhibit extremely

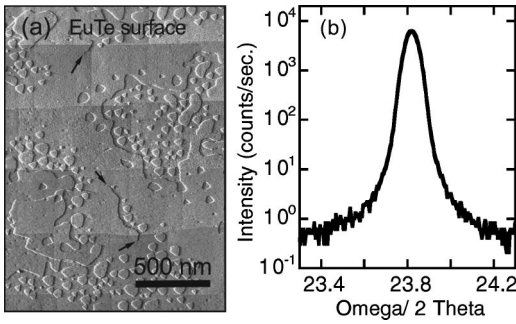


FIG. 1. (a) Scanning tunneling microscopy image of a 3- μm EuTe epilayer surface showing monatomic steps. The arrows indicate threadings of dislocations that penetrate the surface. (b) Rocking curve of the EuTe epilayer before annealing.

smooth surfaces. This is demonstrated by the scanning tunneling microscope (STM) image of a 3- μm EuTe layer shown in Fig. 1(a). The flat surfaces only exhibit monolayer steps that are occasionally terminated by a threading dislocation [arrows in Fig. 1(a)] that results from the growth on the lattice-mismatched BaF₂ substrate. The dislocation density is typically of the order of 10⁸ cm⁻². Also shown in Fig. 1(b) is the x-ray-diffraction rocking curve of the (222) Bragg reflection of a 3- μm EuTe epilayer with a peak position corresponding to the bulk lattice constant. The full width at half maximum (FWHM) of the peak is only 220 arcsec, which indicates a rather good crystalline quality in spite of the lattice-mismatched substrate. The layers also show a clear antiferromagnetic phase transition at the bulk Néel temperature of 9.6 K in SQUID magnetization measurements.¹³

For optical investigations, the EuTe layers were capped *in situ* by a several hundred Å thick BaF₂ protective layer in order to prevent surface oxidation. Magnetoluminescence experiments were performed in a Faraday configuration using a split coil magnet giving fields in the range of 0–8 T. The PL was excited by the 488-nm line of an Ar laser focused on the sample to a spot size of about 100 μm and detected by a photomultiplier with a spectral cutoff at 1.4 eV. The transmission experiments were performed using a 150-W halogen lamp monochromized by a 0.25-m spectrometer.

Typical 1.7-K PL spectra at zero magnetic field are shown in Fig. 2. The luminescence spectra can be divided into two

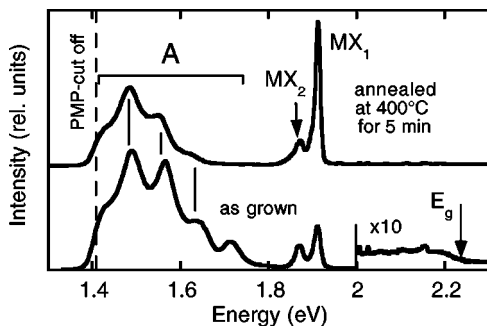


FIG. 2. 1.7-K photoluminescence spectrum of the EuTe epilayer before and after annealing. The arrow indicates the absorption edge and the dashed line denotes the cutoff of the photomultiplier.

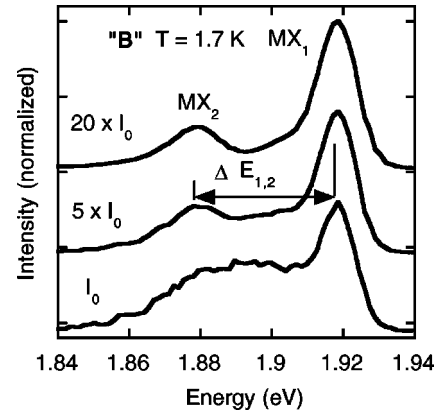


FIG. 3. Luminescence spectra of the annealed sample within band *B* for various excitation intensities ($I_0 = 10 \text{ W/cm}^2$).

regions: a broad luminescence band *A* around 1.5 eV, which corresponds to the PL emission also observed by other groups,^{10,11} and band *B*, which consists of two sharp emission lines close to 1.9 eV. Within the broad PL band *A*, the spectrum exhibits several maxima and minima with a regular spacing of 77 meV. This is due to multiple interference of the PL light within the 3- μm -thick layer. Both emission bands occur at transition energies far below the fundamental absorption edge at 2.25 eV,¹³ which was determined from the high-energy cutoff wavelength of the transmission measurements, and which agrees well with the onset of the PL emission, marked by the arrow in Fig. 2.

At 1.7 K, the PL of our epilayers depends sensitively on the crystalline quality of the samples. This is demonstrated in Fig. 2 by a comparison of the PL spectrum of an as-grown sample with that of a sample annealed at 400 °C for 5 min. As shown in Fig. 2, the post-growth annealing results in a drastic increase of the PL peak intensity of band *B* (I_B), while that of band *A* (I_A) decreases, such that the ratio I_B/I_A increases by a factor of 6. For a set of unannealed samples grown at various substrate temperatures (T_S), we also have studied the PL intensities of bands *A* and *B*. We find the maximum of I_B at a substrate temperature of 355 °C, whereas I_A becomes minimal for this T_S . The ratio I_B/I_A decreases by more than a factor of 2 when T_S deviates by $\pm 15^\circ\text{C}$ from its optimum value. Furthermore, band *A* narrows significantly upon annealing. In heavily doped EuTe epilayers as well as in polycrystalline thin layers, we observe only luminescence from band *A*. This behavior indicates that the broad band *A* is caused by self-activated emission associated with deep centers, as observed also in other wide-gap semiconductors,^{14,15} whereas the lines in band *B* clearly correspond to excitonic transitions. This assignment is in contrast to all previous work on EuTe,^{9–11} where the excitonic emission lines were not observed.

Figure 3 shows PL spectra of the annealed sample within the region of the excitonic emission lines as a function of excitation power I_e . For $I_0 = 10 \text{ W/cm}^2$, we find a narrow emission line at 1.92 eV with a FWHM of only 10 meV, taking into account the monochromator resolution of 5 meV. This sharp line (labeled MX_1) is accompanied by a broader,

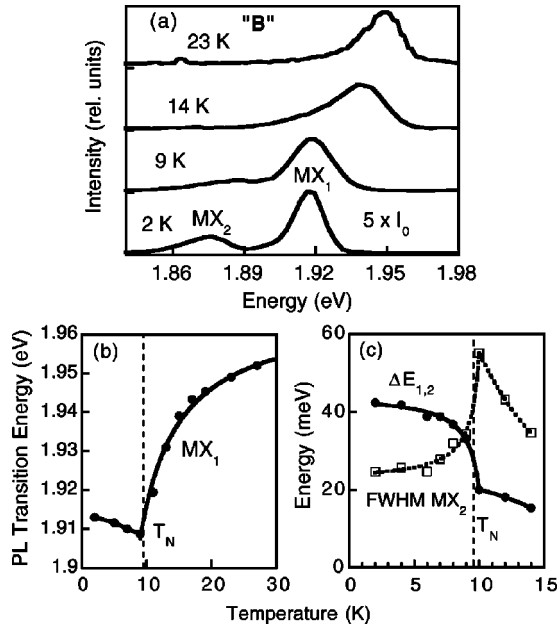


FIG. 4. (a) Luminescence spectra of the annealed sample for different sample temperatures, (b) temperature dependence of the PL transition energy of the main emission line MX_1 , and (c) energy difference between the two emission lines (full dots) and the line-width of the MX_2 peak (open symbols).

50-meV-wide emission centered at 1.89 eV. With increasing I_e , an additional narrow line (MX_2) appears at 1.88 eV. For $I_e > 5I_0$, the PL peak intensity of both narrow lines linearly increases as a function of I_e .

The temperature dependence of the excitonic emission lines is summarized in Figs. 4(a)–4(c). With increasing temperature, the intensity of the MX_2 line rapidly decreases whereas the MX_1 peak at 1.92 eV remains nearly unaffected [Fig. 4(a)]. Below the Néel temperature of 9.6 K, the PL transition energies of both lines are essentially constant or slightly decrease with rising temperature. Above T_N , a rapid blueshift occurs with a total shift of more than 40 meV at 30 K, as shown in detail in Fig. 4(b) for the MX_1 peak. Thus, the magnetic phase transition is directly reflected by a kink in the temperature dependence of the PL transition energies. As shown in Fig. 4(c), at T_N , also a steplike decrease of the energy splitting between the two MX PL transitions occurs, from 33 meV at 9 K to 20 meV at 10 K, together with the appearance of a sharp maximum in the temperature dependence of the FWHM of the MX_2 line at the phase-transition temperature. At 40 K, both exciton emissions are completely quenched.

The most striking feature of the PL emission lines is their huge redshift in applied external magnetic fields (H). As is demonstrated in Figs. 5(a) and 5(b), with increasing field H both excitonic PL lines rapidly shift to lower energies and the splitting between them continuously decreases. The emission energy of the MX_1 peak exhibits a linear magnetic-field dependence [see Fig. 5(b)] even up to the critical field of EuTe of 7.2 T, where the antiferromagnetic-paramagnetic phase transition occurs.¹⁶ From the experimental data, the slope of this redshift is $\Delta E/H = -34$ meV/T, i.e., the lumi-

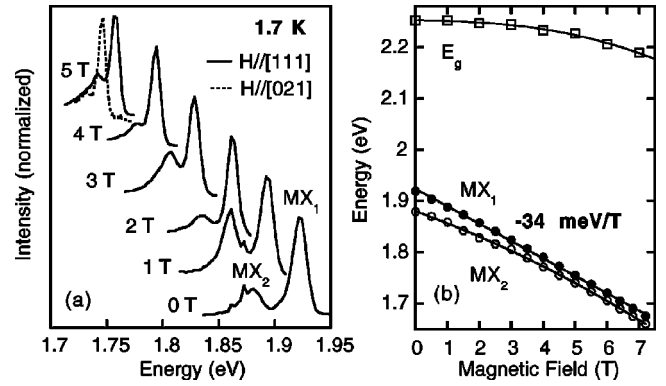


FIG. 5. (a) Luminescence spectra of the annealed sample for various magnetic fields. The dashed spectrum is measured for a different magnetic-field orientation. (b) Absorption edge determined from transmission measurements as well as the observed PL transition energies as a function of magnetic field.

nescence energy can be tuned continuously by more than 240 meV even by a moderate field of 7.2 T. This tuning range is about three times larger as compared to that achieved in all available DMS compounds.

III. DISCUSSION

In DMS, the exciton spin splitting causes a lowering of the band gap with increasing magnetic field. However, the corresponding redshift of the PL emission is considerably smaller than this spin splitting, because it is only equal to half of the spin splitting *minus* the Stokes shift of the PL at zero field due to magnetic polaron formation.⁷ The largest PL shifts are currently obtained in Mn-based ternary II-VI alloys with Mn concentrations above 10%.⁴ For a $Cd_{1-x}Mn_xTe$ sample with $x=0.15$, e.g., we have measured a total PL redshift of 60 meV for $H=7$ T. A slightly larger value may be expected for $Cd_{1-x}Mn_xSe$ due to the higher value of the exchange integrals,⁴ but clearly these values are much smaller as compared to the EuTe case.

For comparison with the results obtained for DMS, it is also useful to define an effective g factor (g_{eff}) by setting the observed magnetic-field shift of the PL energies equal to $0.5g_{\text{eff}}\mu_b H$, where μ_b is the Bohr magneton. With this relation, we obtain a constant $g_{\text{eff}}=1140$ at 2 K for EuTe. While this is comparable to the maximum values for DMS at low fields, for EuTe this g_{eff} is essentially *independent* of H , whereas in DMS it strongly decreases with increasing field. In fact, the field dependence in DMS is given by $1/H$ times a Brillouin function of H . Figure 6(a) shows the temperature dependence of the effective g factor of EuTe, deduced from the MX_1 transition at 5 T. As for the PL transition energies [Fig. 4(b)], a kink in g_{eff} is observed at the magnetic phase-transition temperature, which is slightly shifted to below 9 K because of the reduction of T_N in the applied external field. Within the antiferromagnetic phase, g_{eff} is independent of temperature, whereas for $T > T_N$ (paramagnetic phase), g_{eff} decreases monotonically with rising temperature. In the para-

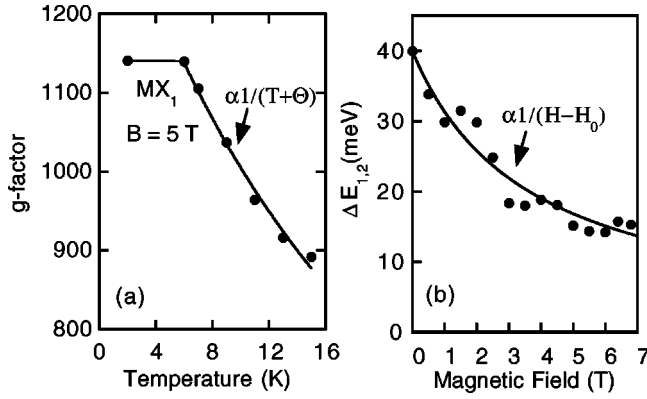


FIG. 6. (a) The effective g factor determined for the MX_1 transition at a magnetic field of 5 T. (b) Energy splitting between the MX_1 and MX_2 emission lines versus magnetic field.

magnetic phase, g_{eff} can be fitted by a Curie-Weiss temperature dependence of $g_{\text{eff}} = C/(T + \Theta)$, giving $\Theta = 24$ K.

There are two further significant differences between the exciton emission in EuTe compared to that in DMS, as shown in detail in Fig. 5(b). First, the EuTe absorption edge is much less magnetic-field-dependent than the PL transition energies (60 meV redshift of the band gap versus 240-meV PL shift at 7 T), whereas the opposite is observed for the DMS. Secondly, the difference between the PL energy and that of the absorption edge (Stokes shift) of 300 meV in EuTe is about 10 times larger as compared to the Stokes shift in II-VI DMS.⁷

Clearly, this large Stokes shift as well as the giant magnetic-field tunability of the PL in EuTe is caused by the formation of magnetic polarons due to d - f exchange interactions between d electrons in the conduction band and electrons localized in the half-filled $4f$ orbitals of the Eu^{2+} ions. The magnetic moment of these polarons is much larger compared to those in Mn-based II-VI DMS because of (1) the localized nature of the photoexcited excitons in EuTe, (2) the higher density of magnetic ions, (3) the larger spin of the magnetic ions ($s = \frac{7}{2}$ for Eu^{2+} compared to $s = \frac{5}{2}$ for Mn^{2+}), and (4), because of the six times smaller antiferromagnetic-exchange coupling between the magnetic ions, which has to be broken up to form magnetic polarons.

This interpretation is supported by recent numerical calculations of optical transitions by Umehara.¹⁷ In these calculations, the spontaneous magnetic ordering of the $4f$ spins and the magnetic polaron formation induced by d - f exchange interactions is taken into account, as well as the Coulomb interaction between photoexcited electron-hole pairs and the electron (hole) -optical-phonon interactions. These calculations predict a distinct temperature dependence of the PL transition energy due to the d - f interaction, with a constant emission energy for temperatures up to T_N , and a subsequent blueshift of 20 meV when the temperature rises from T_N to $2 * T_N$ due to the shrinking of the polaron size. This is exactly the behavior shown in Fig. 4(b), except that the experimental blueshift above T_N is larger than the theoretical prediction. Furthermore, the calculation predicts a linear redshift of the PL transition energy in increasing magnetic

fields, dominated by the d - f interactions, which is again in good agreement with the results shown in Fig. 5(b).

A final point of discussion is the origin of the two excitonic PL peaks MX_1 and MX_2 . At first glance, one would expect these lines to be associated with the emission from localized magnetic polarons, respectively, with emission from polarons trapped to shallow impurities (MX_2). However, the temperature dependence of the MX_2 emission behavior shown in Fig. 4(c) shows that the peak separation between the MX_1 and MX_2 lines rapidly decreases with increasing temperature with a steplike change at the Néel point, accompanied by a pronounced maximum of the PL linewidth. Similar observations have been reported for the luminescence behavior of antiferromagnetic insulators such as BaMnF_4 ,¹⁸ where the luminescence is dominated by interatomic transitions within the Mn^{2+} ions. Thus, our observations are an indication that the MX_2 peak rather represents a magnon side band created by subsequent or simultaneous emission of magnons and photons, an interpretation that is consistent¹⁹ with the measured $1/H$ dependence of the MX_1 - MX_2 energy splitting ($\Delta E_{1,2}$) that is shown in Fig. 6(b). Finally, it is also noted that the magnetic-field-induced redshift of the PL emission in our samples can even be increased by tilting the external magnetic field away from the surface normal direction. This effect could be due to a strain-induced magnetic anisotropy of the layers, which leads to the expectation that in strain-engineered heterostructures of EuTe layers with tailored magnetic anisotropy, the giant PL redshift could be further increased. Also, it is noted that because of the weaker antiferromagnetic f - f coupling, an even larger PL shift than in EuTe can be expected for the antiferromagnetic EuSe.

IV. SUMMARY

In summary, we have demonstrated unique excitonlike photoluminescence emission of high quality EuTe epilayers with giant magnetic-field tunability. The observed PL energy shift of 240 meV at 7.2 T as well as the Stokes shift of 300 meV is by far larger than in any other magnetic semiconductor. In contrast to the diluted magnetic semiconductors, the transition energies of the emission lines vary linearly with magnetic field with a slope of -34 meV/T, and they show a much larger magnetic-field dependence as compared to that of the absorption edge. The magnetic-field dependence as well as the PL blueshift above the magnetic ordering temperature is explained by the formation of large magnetic polarons due to d - f exchange interactions. The giant tunability of the photoluminescence could be utilized for novel magneto-optical devices such as magnetic-field tunable lasers, detectors, and modulators. The huge g factor also provides new possibilities for the development of devices based on spin-polarized carriers such as spin transistors and filters, as has been recently suggested to be used for the realization of spin-based quantum logic elements.²⁰

ACKNOWLEDGMENTS

This work is supported by the FWF, the GME, and the Austrian Academy of Sciences.

- *Electronic mail address: wolfgang.heiss@jk.uni-linz.ac.at
- ¹Y. Ohno *et al.*, *Nature* (London) **402**, 790 (1999).
- ²R. Fiederling *et al.*, *Nature* (London) **402**, 787 (1999).
- ³J. S. Moodera, R. Meservey, and X. Hao, *Phys. Rev. Lett.* **70**, 853 (1993).
- ⁴For reviews, see, e.g., J. K. Furdyna and J. Kossut, in *Semiconductor and Semimetals*, edited by R. K. Willardson and A. C. Beer (Academic Press, New York, 1988), Vol. 25; T. Dietl, in *Handbook on Semiconductors*, edited by T.S. Moss (North-Holland, Amsterdam, 1994), Vol. 3b, p. 1251.
- ⁵E. L. Nagaev, *Pis'ma Zh. Éksp. Teor. Fiz.* **6**, 484 (1967) [*JETP Lett.* **6**, 18 (1967)].
- ⁶*Phys. Kondens. Mater.* **11**, 231 (1970).
- ⁷G. Mackh *et al.*, *Phys. Rev. B* **50**, 14 069 (1994).
- ⁸H. Togashi *et al.*, *J. Phys. Soc. Jpn.* **57**, 353 (1988).
- ⁹G. Busch, P. Streit, and P. Wachter, *Solid State Commun.* **8**, 1759 (1970).
- ¹⁰P. Wachter, *Crit. Rev. Solid State Mater. Sci.* **3**, 189 (1972).
- ¹¹R. Akimoto, M. Kobayashi, and T. Suzuki, *J. Phys. Soc. Jpn.* **63**, 4616 (1994).
- ¹²G. Springholz and G. Bauer, *Appl. Phys. Lett.* **62**, 2399 (1993).
- ¹³H. Krenn *et al.*, *Phys. Rev. B* **60**, 8117 (1999).
- ¹⁴A.N. Georgobiani, S.I. Radautsan, and I.M. Tiginyanu, *Fiz. Tekh. Poluprovodn.* **19**, 193 (1985) [*Sov. Phys. Semicond.* **19**, 121 (1985)].
- ¹⁵P. Hacke, H. Okushi, T. Kuroda, T. Detchprohm, K. Hiramatsu, and N. Sawaki, *J. Cryst. Growth* **189-190**, 541 (1998).
- ¹⁶H. Hori *et al.*, *Physica B* **201**, 438 (1994).
- ¹⁷M. Umehara, *Phys. Rev. B* **52**, 8140 (1995).
- ¹⁸T. Tsuboi and W. Kleemann, *Phys. Rev. B* **27**, 3762 (1983).
- ¹⁹R. Merlin *et al.*, *Solid State Commun.* **22**, 609 (1977).
- ²⁰D. P. Vicenzo, *J. Appl. Phys.* **85**, 4785 (1999).